Current Science
CS 5 (1), 1353– 1365 (2025)
Received 10 **Dec** 2024 | **Revised 16 Jan** 2025 | **Accepted 05 Feb**. 2025 | **Online Available 20 Feb** 2025
https://doi.org/ 10.52845/CS/2025-5-1-30

Current Science

Current Science

OPEN ACCESS

ISSN(O)2795-8639

ORIGINAL ARTICLE

Design, Modelling and Test on an Energy Harvesting Treadmill with Flexible Damping and Wireless Sensing

Mingyue Li[a], Qianwen Wu[a], Qi Wang[a], Zhengwei Yang[b] and Dong Guan[a*]

[a]College of Mechanical Engineering, Yangzhou University, Yangzhou, China;

[b]China North Vehicle Research Institute, Beijing, 100072, China

[*]Corresponding Author: Dong Guan

Abstract

An energy harvesting treadmill is proposed in this study, exhibiting several advantages (e.g., damping adjustable, self-power wireless sensing, as well as real-time monitoring). The compact configuration of the connected treadmill is proposed for its energy harvesting property, and a mechatronic damper is employed to replace the conventional hydraulic damper. Subsequently, the kinematic principle of the energy harvesting treadmill is investigated through virtual prototyping. Next, the compression and rebound process are analyzed comprehensively. Lastly, the experimental test is performed to explore the dynamic property of the mechatronic damper as well as the conventional damper. The damping force can be regulated flexibly and electronically by varying the external resistor properly. Moreover, the energy harvesting property is confirmed. The results suggest that the extracted energy is at a 10W level, which can power the wireless connector system. The exercise process can be monitored through the developed APP, without an extra power supply or battery.

Keywords: Treadmill; Mechatronic damper (MD); Resistance adjustable; Internet of Things; Condition monitoring.

Introduction

Treadmills are essential device for disease therapy [1], rehabilitation training [2], and fitness [3]. To adjust the resistance, a conventional treadmill needs extra mechatronic devices, which leads to several disadvantages (e.g., complex structure, high cost, low reliability, and extra energy consumption).

As the Internet of Things (IoTs) has been leaping forward, a health monitoring device powered by human motion (i.e., sports energy) turns out to be a booming area [4-7]. For instance, an energy harvesting backpack for outdoor sports is developed with a mechanical device to convert the motion of the suspended load into a unidirectional rotating shaft of the generator [8]; or extract negative work [9]. To extract energy, portable or wearable electronic devices are developed considering biomechanics and so forth. [10-12], the above-mentioned all provide novel insights into energy harvesting in sports areas. Energy harvesting efficiency is also an important indicator. At present, with the continuous advancement of energy harvesting component technology, the power output of wearable devices has been rising [13-14], and the dynamic performance of energy recovery devices has been enhanced progressively [15-17].

In terms of the energy harvesting mechanism, there are piezoelectric [18], electromagnetic [19,20], triboelectric methods [21-23], and so forth. Human motion has the nature of low-frequency and irregular; all the above-described three approaches can be adopted to extract the relevant kinetic energy. 300 μW-2.5 mW power can be extracted using the EMG designed by Saha [20] Though effective to power a single sensor, it is too smaller to power consumer electronics (e.g.,

a smartphone).

In brief, the state-of-art of the current treadmills exhibits the following properties:

- Dynamic performance of the conventional treadmill with passive hydraulic damper is sensitive to the environmental temperature, stiffer at high while softer at low temperature, due to the viscosity variation of hydraulic oil. Besides, leakage could occur without a long duration.
- The resistance is regulated by extra mechatronic circuits and actuators, such that it is subjected to several disadvantages (e.g., being complex in structure, high in cost, low in reliability, and waste energy).
- The current energy harvesting from human motion is effective, whereas the power is at the mW level, which should be boomed. Accordingly, to power, the health monitoring sensors are employed, and the wireless communication is achieved.

The motivation of this study is to propose a mini treadmill to overcome the drawbacks summarized before. In general, the main contributions of this study are:

- A smart treadmill is developed in accordance with the energy harvesting mechatronic damper (MD). To be specific, the damping force can be regulated electrically to fit objects with different weights and a wide range of requirements.
- The energy harvesting circuits is proposed, it consists of rectification, filter, energy storage and wireless communication modules. The energy harvesting circuits are proposed, it consists of rectification, filter, energy storage, and wireless communication modules.
- The wireless interface is developed and packaged, and the real-time voltage and power can be monitored wirelessly through the intelligent terminal.
- Whole system is self-powered by human motion, without extra battery or power supply, and the scarved power is at 1-10 W level.
- The rest of this study is organized as follows. In Section 2, the schematic design and prototype are illustrated, especially for mechatronic dampers. In Section 3, the overall virtual prototyping is developed, and the kinematics analysis is conducted. In Section 4, the damping performance of mechatronic and conventional hydraulic dampers is examined. Furthermore, the demo test is provided as well. In Section 5, conclusions and remarks are presented.

2. Structure Design and Operational Principle

2.1 Structure Design of the Treadmill

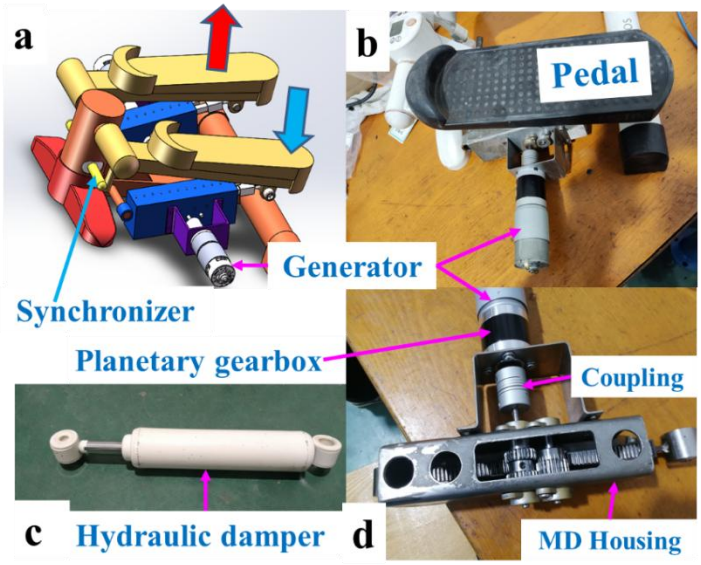

Figure 1 The treadmill (a)3D model; (b)Fabricated prototype; (c)Conventional hydraulic damper; (d)The developed mechatronic damper.
(Red arrow: rebound process; Blue arrow: compression process)

Fig. 1 illustrates the proposed mini treadmill and its key components. Fig. 1(a) presents the schematic configuration using the 3-dimensional model. At the top of the mini-treadmill, there are two pedals supporting the user's body. When the treadmill is employed, one foot moves downward (blue arrow), whereas the other moves upward (red arrow). Both pedals sway simultaneously under the displacement constraint imposed by the synchronizer, which is embedded in the vertical frame while conforming to a space-constrained revolute joint. The pedal is suspended under two revolute joints. The front of the pedal is coupled with the treadmill frame, and it exhibits one degree of freedom (DOF), while the pedal end is connected with the damper through the revolute joint. The motion of the pedal end comprises two DOFs. To be specific, one is rotation along the connection pin, and the other is along the vertical direction.

For the conventional treadmill, a hydraulic damper connects with the pedal end, and the other end rotates with the frame of the treadmill parallelly. The cylinder block of the damper rotates with the frame, whereas the motion of the damper rod comprises rebound/compression, and rotation with the pedal end. The hydraulic damper is subjected to several disadvantages (e.g., being sensitive to the environment, leakage, and damping non-adjustable). Hence the treadmill is stiffer in winter while softer in summer, inherent reason is that the hydraulic oil viscosity varies with temperature while the orifice size is tiny. Furthermore, the relief valve size is fixed, it can only fit users with a narrow weight range. To address the above-described issues, a damping adjustable mechatronic damper is proposed (Fig. 1(d)), comprising a rack, three spur gears, a coupling, as well as a gear motor.

2.2 Structure and Operational Principal of the Mechatronic Damper

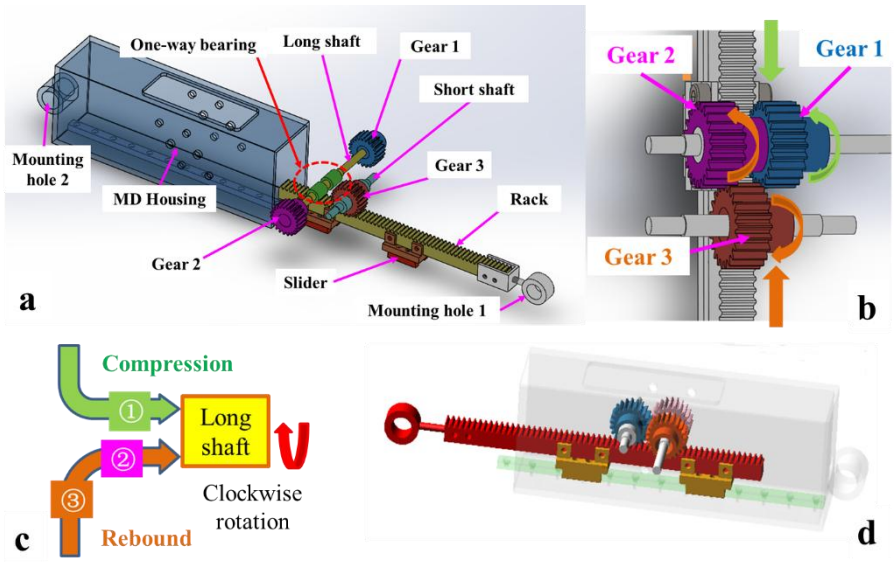

Figure 2 The mechatronic damper (a)Transmission mechanism; (b)Motion rectifier mechanism; (c) Power flow; (d) Virtual prototyping.

Fig. 2(a) depicts the structural details of the mechatronic damper, comprising a housing, a rack, two sliders, a linear guide, two one-way rolling bearings, three spur gears, two connectors, two shafts, and four bearing seats, as presented in Fig. 1(d). The bearing seat is screwed on the mechatronic damper housing. Both ends of the respective shaft are suspended by the bearing. The bottom of the housing is perforated and then tapped to mount the linear guide rail. Accordingly, the internal bottom surface is milled to ensure installation accuracy. The linear guide rail is screwed and then fixed on the housing as well, and the slider slides on the guide rail to transfer the sliding friction to rolling friction, reduce the energy loss and improve system efficiency and durability. Sliders and rack move synchronously due to the connectors, which are screwed on the sliders and rack, respectively.

There are two gears mesh with the rack (i.e., gear

1 and gear 3). Besides, gear 2 is only driven by gear 3. Notably, gear 1 and gear 2 are located on the long shaft through the one-way bearing, with the ultimate purpose of achieving the motion rectifier purpose. The gear 1 and the gear 2 serve as boss gears with 10 inner holes of 22 teeth of 1 mold, and gear 3 acts as a boss gear with 6 inner holes of 22 teeth of 1 mold. The movement range of the rack reaches 50mm.

In the compression process, the rack moves along the green arrow direction, gear1 engages with the long shaft, which rotates clockwise (from right to left); gear 3 mesh with the rack and rotates clockwise, the power is subsequently transferred to gear 2, which rotates anticlockwise. Under one-way bearing, gear 2 rotates idly, whereas it does not engage with the long shaft. In the rebound process, gear 1 rotates idly and anticlockwise (from right to left), it disengages with the long shaft due to a one-way bearing. Gear 3 rotates anticlockwise (from right to left). Subsequently, the power is transmitted to gear 2, which rotates clockwise (Fig .2(b)). Gear 2 engages with a long shaft and motion power is delivered to the generator by a long shaft.

Thus, no matter how the rack vibrates up and down, the motion is transmitted through long shaft 2, and always clockwise. Fig. 2(c) presents a schematic diagram of the power flow.

The selected motor must be compact and light to consider the installation location. The generator is required to exhibit low rotor inertia and high rotation speed to enhance efficiency. Accordingly, the brushless DC motor is selected, and a gearbox is integrated into the motor to make sure the generator operates at a relatively high speed.

The planetary gearbox is capable of supplying a larger transmission ratio, such that it can generate large damping torque and obtain higher power output. On that basis, the selected motor model refers to a 42XA775 planetary gear motor, with the parameters listed in Table 1.

Table 1: 42XA775 planetary gear motor parameters

Parameter	Value
Voltage	24 V
Current	0.6 A
Power	35 W
No-load speed	200 r/min
Load moment	4.01 kgf·cm
Load speed	175 r/min
Motor size	42*(L+66)mm
Shaft size	8*23 mm

The damping force of the damping system can be dynamically regulated, and the damping force can be regulated by changing the resistance value. The damping force is controlled according to the following formula [21]:

$$F = \frac{K_t K_e}{r\left(R_L + R_a\right)} \omega i_g \qquad (1)$$

where F is the damping force, Kt is the torque constant of the generator; Ke is the back electromotive force constant of the generator; ω is the speed of the motor, rad/s; ig is the gearbox transmission ratio; and RL is the external variable resistance of the generator; Ra represents the equivalent resistance of the armature of the generator, and r is the radius of the gear connected with the one-way clutch.

3. Virtual Prototyping Simulation and Analysis

3.1 The Establishment of Virtual Prototype

In this section, a virtual prototyping model of the proposed treadmill is established to capture dynamic properties the prototype.

Table 2. Motion constraints

Constraint pair	Part 1	Part 2
Contact	Rack	Gear1
Contact	Rack	Gear3

Script control	Gear1	Long shaft
Contact	Gear1	Gear2
Script control	Gear2	Long shaft
Script control	Gear3	Short shaft
Fixed	Coupling	Long shaft
Fixed	Coupling	Generator
Fixed	Slider	Rack
Contact	Slider	Guide rail
Revolute	Mounting hole 1	Pedal
Revolute	Mounting hole 2	Pedestal
Revolute	Pedestal	Synchronizer
Revolute	Pedal	Pedestal
Contact	Pedal	Synchronizer

Motion logic is quite important to the treadmill prototype, it impacts the operational functions and practical comfort. Thus, the motion constraints of the whole prototype are illustrated in Table 2.

The boundary conditions fall into two portions, i.e., the motion logic of the whole treadmill and the internal motion principle of the damper. As depicted in Fig. 1a, the energy harvesting damper exhibits one degree of freedom (1-DoF), manifested by reciprocating extension and compression. All motion parts in the prototype only exhibit 1-DoF, such that the pedal and pedestal connect through the revolute joint, with the aim of ensuring the basic motion of the pedal. The pedal and the synchronizer are constrained with contact pair, with the aim of coordinating the motion of two pedals and the motion amplitude. It is noteworthy that the synchronizer is embedded in the pedestal with a revolute joint, rotating in a limited domain following the sway of the pedals.

As presented in section 2, the front and end mounting holes of the mechatronic dampers are connected using revolute joints. Gear 1 and 3 are contacted with a rack. Subsequently, gear 2 comes into contact with gear. Gear 1 and gear 2 engage with a long shaft based on script control, under the operational logic of a one-way clutch. The kinetic energy is exported by the long shaft, gears in the planetary gearbox come into contact with each other, and finally to the rotor shaft of the generator, such that a magnet is embedded on its surface. Moreover, the rotating magnetic field is cut by stator coils. With the increase of the generator speed, the damping force will be enhanced, as expressed in Eq. (1), the output voltage will be increased, and the generator efficiency will rise. Fig. 2(d) illustrates the simulated damper virtual prototyping. Although it has extra damping force during operation, i.e., inertial and friction force, the above-mentioned forces are small compared with the electromagnetic force generated by the motor. Accordingly, in the simulation process, only the electromagnetic force generated by the motor is considered.

3.2 Simulation Results and Discussions

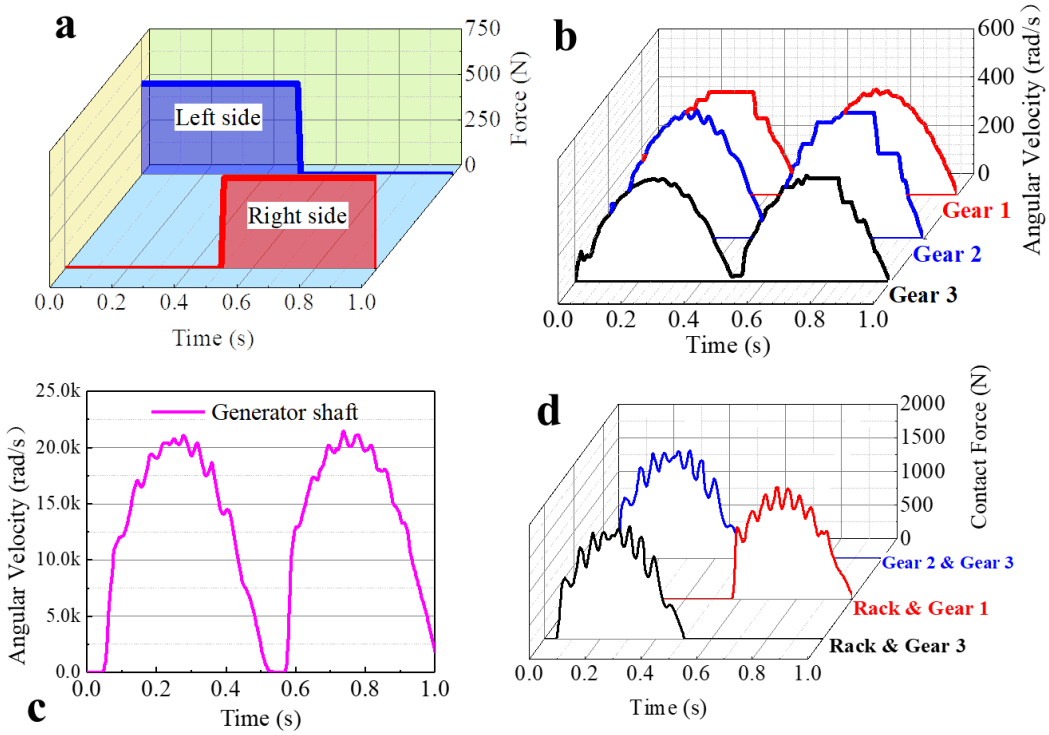

Figure 3 The simulated (a) Pedaling force; (b) Velocity of gears 1-3; (c) Velocity of generator shaft; (d) Contact force between gears and rack (right damper).

Fig.3 illustrates the simulated kinematic and dynamic properties. The pedal force refers to the input of the whole system. The following assumptions are considered:

- The weight of the customer reaches 50 Kg.
- The inertia effects during operation are neglected.
- The pedal force is a constant and loaded persistently.
- The operation frequency is 1 Hz.

Thus, the applied load can be found in Fig. 3(a), from 0 to 0.5s, the left pedal is downward, and the total mass of 500N is loaded on it. Due to the motion constraints, the damper under the left pedal is compressed, while under the right pedal is extended, both generate the mechatronic damping simultaneously. From 0.5 to 1s, the right pedal moves downward, whereas the left is upward, and the right damper is compressed while the left one extends. Next, a new cycle begins. The and are set to 0.35 and 137 respectively. The angular velocity of gears 1, 2, and 3 are demonstrated in Fig. 3(b), it reveals that all three gears rotate no matter compression or extension process. Furthermore, the maximum speed is nearly 430 rad/s. Fig. 3(c) presents the angular speed of the generator shaft, enlarged by the planetary gearbox at a maximum speed of 21000 rad/s, which is about 48 times larger than the rotation speed of gears 1 and 2, the magnification is the transmission ratio of the gearbox. The ultimate purpose is to enlarge the damping force, as well as the output efficiency of the generator.

Fig. 3(d) presents the contact force between the rack and different gears. Notably, the damper is mounted on the right pedal, such that it is rebound (0-0.5 s) first and compressed between 0.5 and 1s. As depicted in Fig. 2(c) and 3(d), the power flow can be elucidated as follows:

From 0 to 0.5s, gear 3 is driven by rack extension, gear 3 meshes with gear 2, such that the kinetic energy is transferred to the long shaft. It is noteworthy that though gear 1 rotates, gear 1 will not engage with the long shaft under the one-way clutch effect, such that it rotates idly from 0 to 0.5s.

The damper is compressed between 0.5 and 1s. Accordingly, rack meshes with gear 1, such that the power is transferred to the long shaft directly. Simultaneously, gear 3 meshes with rack and gear 2 in sequence. However, under the one-way clutch mounted between gear 2 and the long shaft, gear 2

and gear 3 rotate idly, i.e., the inherent reason that contact force between rack & gear 3, gear 2 & gear 3 declines to 0, whereas their angular speed is synchronized with gear 1.

The weight range of the stepping machine applies to the weight of most adults (50-80kg). The gravity applied is set as 500N and 800N respectively, in Adams simulation. Fig. 4 presents the comparison of its damping force in half a cycle. Weight fluctuations exerts a slight effect, and the stepping machine can bear the weight of most adults.

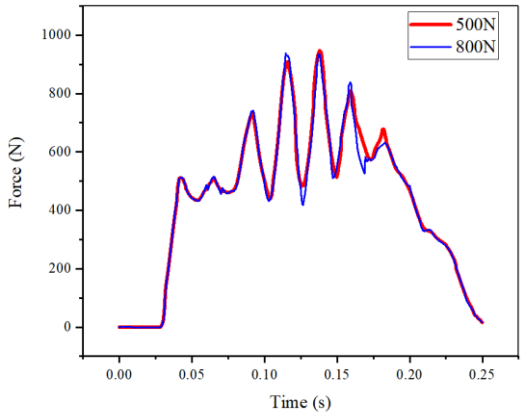

Figure 4. Damping force at 500N and 800N loads.

As revealed by the result in Fig. 2 and 3 and the above discussions, the designed mechatronic damper is effective, and the motion logic is reliable. All the rotation parts move based on the half-sine wave under the persistently applied load, arising from the motion logic of the treadmill prototype that the pedal phase is shifted alternatively. The small saw-tooth waveform occurs in accordance with sine-wave configuration. The reasons for the above result are inferred (e.g., the nonlinear contact effects among rack and different gears, the nonlinear friction effects between different contact parts, as well as the dynamic equilibrium effects between human motion input and the electromagnetic damping resistances).

Experimental results

4.1 The test bench

In the present section, damping and energy harvesting performance of the prototype are examined, the bench and on-site tests are performed at the NVH (Noise, Vibration and Harshness) laboratory of Yangzhou University.

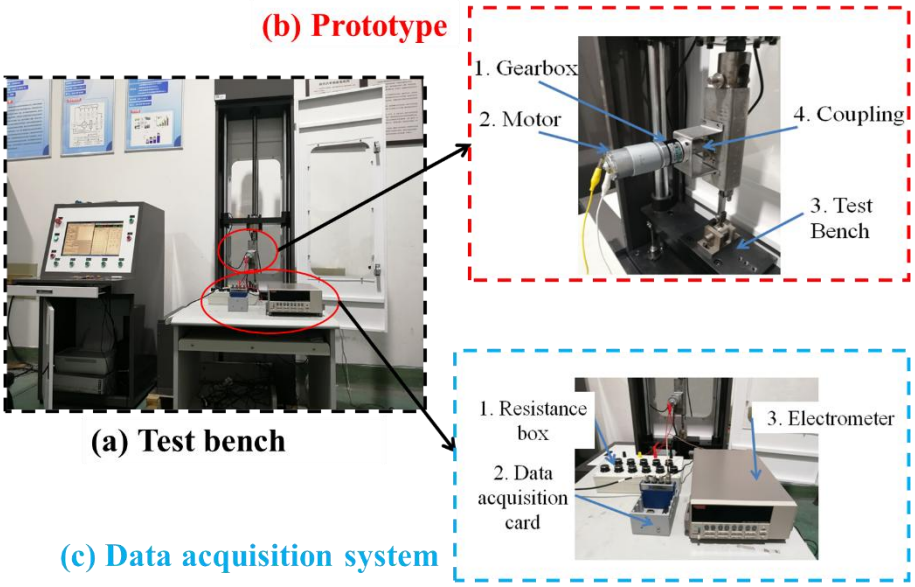

Figure 5 Test bench and prototype of the mechatronic damper

Fig. 5 presents the test bench and fabricated prototype. For the test bench, which consists of the control system and loading system, a slider-crank mechanism is applied to excite the damper displacement, a servo motor is utilized to power the crank, whose length is adjustable. Both displacement and force sensors are employed to collect the dynamic displacement and damping force of the damper. To be specific, the upper mounting hole of the energy recovery device is fixed by a pin, and the lower mounting hole on the rack is clamped on the test bench with a special clamp, and the rack is excited up and down. Thus, the indicator diagram at a range of frequencies and external loads can be acquired, and the damping characteristic curve can be more directly identified in accordance with the diagram.

Fig. 5 presents the produced prototype and test bench, comprising the excitation source, displacement sensor, force sensor, and shock absorber indicator fatigue comprehensive test bench. To be specific, the upper hanger ring of the shock absorber is clamped through the clamp, its lower hanger ring and rack are clamped on the bench through the special clamp, and let its upper shell is pulled up and down. The amplitude is regulated on the shock absorber indicator fatigue comprehensive test bench. Next, the vibration frequency on the computer is set. Subsequently, the start key is pressed, and the tension of the shock absorber will be displayed on the computer. In electrical experiments, the resistance box is directly connected to both ends of the motor, and the electrometer and data acquisition card are connected to the resistance box in parallel.

In the indicator diagram of the bench test of the energy recovery device, when the displacement varies in the positive direction, suggesting that the prototype is in the stretching stroke. Moreover, when the displacement changes in the reverse direction, it is in the compression stroke.

4.2 The Examined Dynamic Properties

Accordingly, a rated 200r/min, 24V motor is employed as the generator of the damper, details of the motor parameters can be found in table 1. The excitation amplitude and frequency are 20mm, 0.5Hz and 1Hz respectively. The examined damping characteristics can be found below.

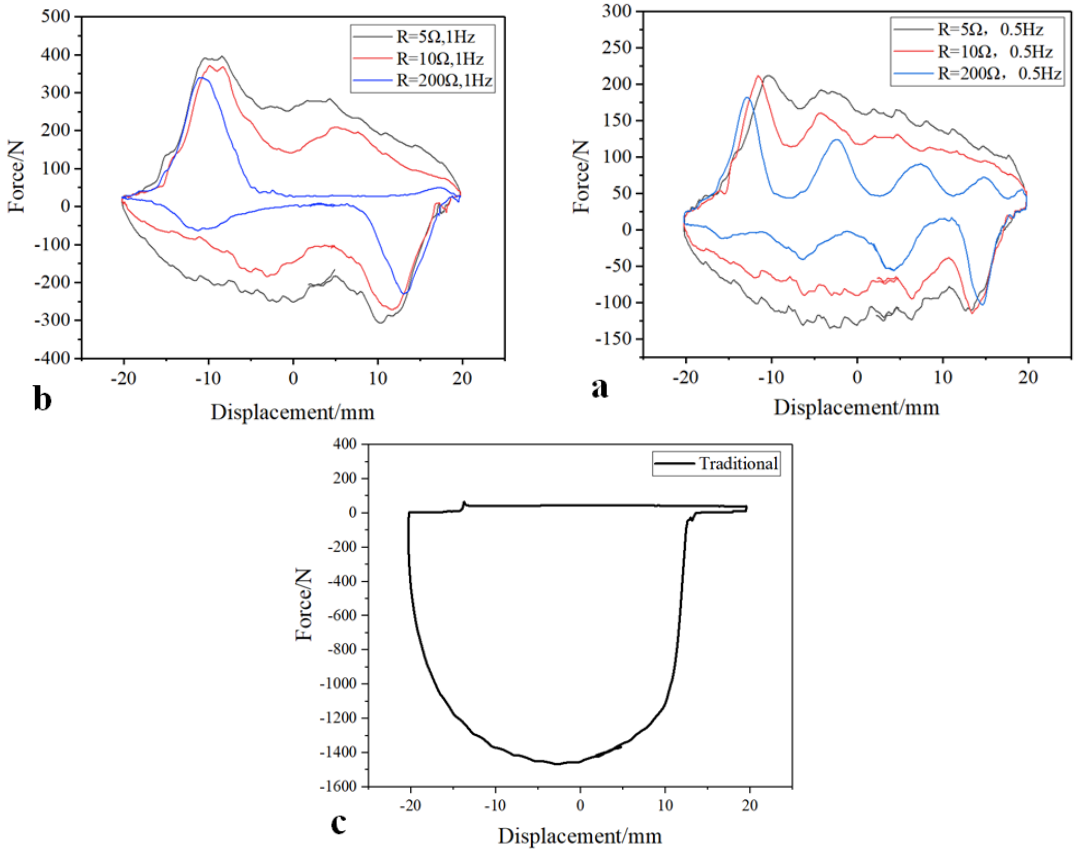

Figure 6 The damping performance under 20mm excitation amplitude (a) 0.5 Hz; (b) 1 Hz; (c) conventional hydraulic shock absorber

It can be found from Fig. 6 that the damping force of this prototype is proportional to the excitation frequency. As the frequency increases, the damping force increases accordingly. For example, at 0.5 Hz, the maximum damping force is about 200 N with 5 Ω external resistance. While the maximum damping force can enhance to 400 N when the excitation frequency is 1Hz. The damping force of this prototype is inversely proportional to the external resistance. As the resistance increases, the damping force decreases accordingly. Furthermore, the supplied damping force fluctuates seriously with a larger resistance. As depicted in Fig. 6(a), the damping curve fluctuates from 50 N to 150 N under the external resistance of 200Ω, which is unstable and does not fall into a scope of the expected phenomenon. An inherent reason is expressed in Eq. (1), and the damping force is limited due to high resistance, such that dynamic equilibrium between pedal force varies dramatically. First, a smaller pedal force results in the large acceleration of the generator rotor, the suddenly enhanced rotor speed subsequently generates a larger damping force, which inversely enhances the total pedaling resistance and decreases compression/extension speed. In general, electromagnetic damping force fluctuates with generator speed, which is impacted by the coupling effects of pedal force and external resistance.

Waved damping force does not act as the desired operation condition, since it is harsh and impacts comfort. The ideal damping force occurs when external loads decrease, a fuller indicator diagram exists in Fig. 6(a) when the external load decreases to 5Ω. This means the damping force is more stable and persistent during the whole operation process. In Fig. 6(b), the excitation frequency is enhanced to 1Hz, while the excitation amplitude is 20mm as well. The damping force is about 2 times larger than 0.5 Hz. For the conventional hydraulic damper, which is illustrated in Fig. 1(c), its damping characteristic is also examined and displayed in Fig. 6(c). The hydraulic damper is only effective in the compression process, while the damping force on extension is 0 N. In other words, only the downward pedal supply damping force if the treadmill is equipped with a hydraulic damper, while the proposed mechatronic damper is effective bidirectionally. Thus, the damping of the proposed treadmill prototype is more fluent and persistent.

When the shock absorber starts from the static state, or from the bottom dead center starting to move, the relative error between the practical and theoretical value is large. The major reason for the above result is the dynamic response of the shock absorber at the beginning of movement, that is, the transmission parts of the shock absorber will produce elastic deformation in the process of acceleration, and the energy accumulated by this elastic deformation will be released with the decrease of acceleration. Accordingly, the indicator curve of the shock absorber will produce large fluctuations when starting movement and reversing. When the shock absorber runs smoothly, the dynamic response decreases gradually. This is an unavoidable phenomenon in dynamic system, and relevant researchers have also appeared the above-mentioned phenomena[22]. We are in the process of studying how to mitigate the dynamic response phenomenon by controlling the external resistence. From Fig. 6(a) and Fig. 6(b), there will be some sawtooth fluctuations in the measured indicator diagram, which is caused by the collision between moving parts in the internal structure when the shock absorber works. Changing the gear and rack with smaller modulus and adding lubricating oil between the gear and rack can improve the situation.

4.3 The Examined Electrical Properties and Demonstrations

The electrical characteristics was examined in the NVH laboratory of Yangzhou University. The test bench and data acquisition system can be found in Fig. 4, the equipment models are as follows: test bench (TPJ-W5A), NI data acquisition system (9174-9223), electrometer (6154).

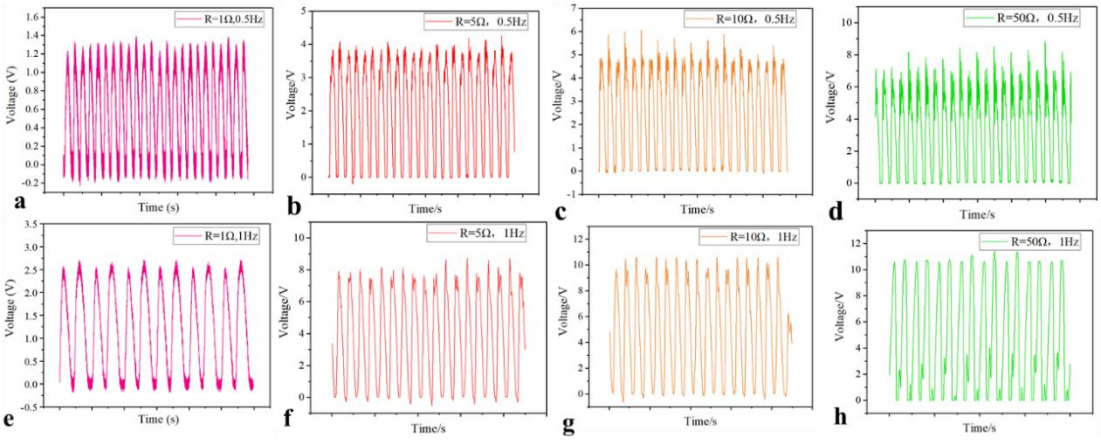

Figure 7 The voltage generated by mechatronic damper (a) R=1Ω, f=0.5Hz; (b) R=5Ω, f=0.5Hz; (c) R=10Ω, f=0.5Hz; (d) R=50Ω, f=0.5Hz; (e) R=1Ω, f=1Hz; (f) R=5Ω, f=1Hz; (g) R=10Ω, f=1Hz; (h) R=50Ω, f=1Hz. (Excitation amplitude 20 mm)

The extracted voltage under different external loads and excitation frequencies are illustrated in Fig. 7. In Fig. 7(a)-6(d), the excitation frequency is 0.5Hz, while in Fig. 7(e)-6(h), the excitation frequency is 1Hz; the connected external resistance is 1Ω, 5Ω, 10Ω and 50Ω, respectively.

In Fig. 7(a), the extracted maximum voltage is nearly 1.3V. Besides in Fig. 7(d), the generated voltage reaches up to 7V. The only difference between Fig. 7(a) and 7(d) lies in the value of series resistor. The internal resistance of the generator coil, Ra, reaches 3-4 Ω, such that the total resistance in Fig. 6(a) is nearly 3-5 Ω, whereas the total resistance in Fig. 7(d) reaches 53-54 Ω. The current in Fig. 7(a) is significantly larger than the current in Fig. 7(d). Ampère's force law and the above-described inference reveal that the damping force with smaller external resistance should be larger. The damping force is inherently generated in accordance with Ampère's force law, F=BIL, where B denotes the strength of the magnetic field. It is fixed for a specific generator, since the permanent magnet and its configuration are specific, consistent with effective coil length L. Thus, the only variation is the coil current, I. With the increase of the generator speed, the generated current will be increased, and the examined voltage will rise. The above conclusion can be drawn through the comparison between Fig. 7(a) and 7(e), which have the only difference in excitation frequency, 0.5Hz and 1Hz respectively, under the identical excitation amplitude, 20mm. Notably, the compression/extension speed of the mechatronic damper is higher under 1Hz excitation, such that it obtains a larger coil current. As a result, a higher examined external circuit voltage is generated, nearly 2 times enlarged. In the laboratory, a 70kg adult is invited to move on the treadmill at a normal frequency, and the output current of the treadmill is measured using the electrometer. After DC/DC module rectification, the result is presented in fig. 8, i.e., the voltage ranges from 4 to 6V.

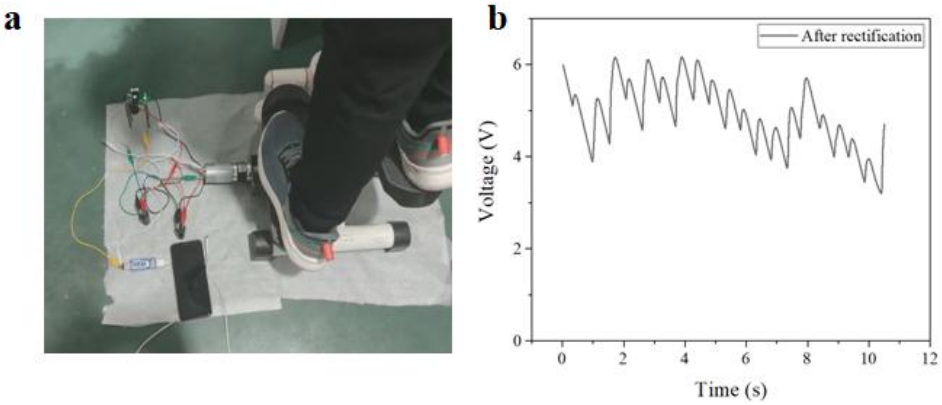

Figure 8 (a) Normal step condition; (b) Output voltage after rectification

The voltages displaced in Fig. 7 suggest that though it is the direct current (DC), the serious fluctuation restricts its direct applications. Accordingly, a rectifying filter circuit is required to improve the output quality, with the aim of conforming to the basic requirement of consumer electronics (e.g., smartphones and intelligent terminals). Fig. 9 presents the effective solutions, in which the generated power is stored in the super capacitor series first to decrease the sharp fluctuations. The capacitor module covers 6 capacitances, whose capacity and voltage reach 1000 μF and 50 V, respectively. Subsequently, the storage power is regulated using a DC-DC module, which is based on the LM2596 chip. The DC output can be regulated among 3.3V to 33V. Lastly, the regulated DC power falls into two portions. To be specific, one is the output module with a USB port, which can be employed to power intelligence terminals; the other is the Bluetooth module, which is exploited to achieve wireless communications. Both the schematic and prototypes are presented in Fig. 9.

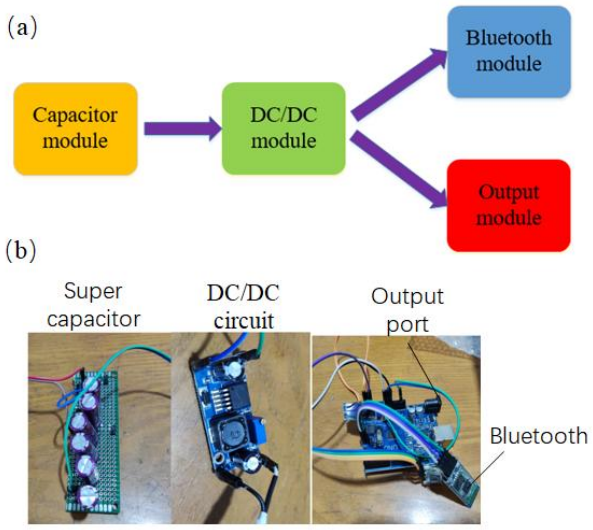

Figure 9 Energy recovery circuit (a) Schematic diagram ;(b) Physical circuit.

Figure 10 (a) On-site test; (b) Bench test; (c) Charging cell phone; (d) Wireless communication interface

Both the on-site tests and bench tests on conducted, which are illustrated in Fig. 10. In Fig. 10(a), the kinetic energy from the treadmill user is transferred to electrical power through the fabricated mechatronic damper; Fig. 10(b) illustrated the identical test system, the difference is an input energy source, it is driven by the test bench. Beyond the energy harvesting circuit, a powered cellphone and wireless connected intelligence terminal are also displayed. Details can be found in Fig. 10(c), which demonstrates the cellphone can be charged persistently Besides, the self-powered Bluetooth system can communicate effectively and rapidly after the mechatronic damper work, as shown in Fig. 10(d). Three indicators can be collected in the APP interface, which is charge current, charged power, and the harvested energy respectively. The APP interface is coded based on the E4A development environment. Thus, the excise conditions can be monitored under totally self-power and wireless ways. More details can be found in the supplementary videos.

Conclusion

In this study, an energy harvesting treadmill is proposed, exhibiting several advantages (e.g., damping adjustable, self-power wireless sensing, and real-time monitoring). The critical component of the damping flexible treadmill refers to the mechatronic damper, whose damping force can be regulated flexibly by varying the external resistance electronically. Accordingly, disadvantages of the conventional hydraulic-equipped treadmill can be overcome properly (e.g., leakage, fixed damping, and sensitive to temperature). Both virtual prototyping and experimental test are conducted to validate its effectiveness, and the extracted energy from the human treadmill can be up to 10W. An energy harvesting circuit is developed for matching with the fabricated treadmill hardware, the circuit comprises three modules, i.e., are the capacitor module, DC-DC module, and wireless module respectively. Furthermore, an APP interface is developed to achieve the wireless connection on the intelligent terminals. The proposed treadmill is more flexible and friendly for disease therapy, rehabilitation training, as well as fitness.

Statements and Declarations

Funding This work is funded by the Natural Science Foundation of China (Grant No. 52005433), Special Cooperation Foundation for Yangzhou & YZU (No. YZ2022202), Jiangsu Association for Science and Technology "Young Talent Support Project" (2021037) and International Science and Technology Cooperation Projects of Yangzhou & YZU (No. SGH2023000013).

Conflict of Interest The authors declare that they have no conflicts of interest relevant to the content of this article.

Ethics Approval Not applicable.

Consent to Participate Not applicable.

Data availability Not applicable.

Code availability Not applicable.

Contribution Statement Substantial contributions to conception and design: D Guan. Experimental test and prototype simulation: QW Wu and D Guan. Drafting the article or revising it critically for important intellectual content: D Guan, QW Wu and ZW Yang. Final approval of the version to be published: D Guan, QW Wu and ZW Yang.

References

1. Slysz J, Lu T, Zhao LH et al (2020) Treadmill Exercise Training Reduces the Systolic Blood Pressure Response to Walk Exercise in Patients With Peripheral Artery Disease. Circulation 142(3): A14290.
2. Pamela W D, Katherine J S, Andrea L B et al (2020) Body-weight–supported treadmill rehabilitation after stroke. New Engl J Med 364: 2026-2036.
3. Kyle M, Serge H, Paul Cremer et al (2018) Association of Cardiorespiratory Fitness With Long-term Mortality Among Adults Undergoing Exercise Treadmill Testing. JAMA Netw Open 1(6): e183605.
4. Wang HF, Seifedine N K, Ebin D R (2020) Continuous health monitoring of sportsperson using IoT devices based wearable technology. Comput Commun 160: 558-595.
5. Giorgio B, Paolo C, Laura F et al (2018) Human activity monitoring system based on wearable sEMG and accelerometer wireless sensor nodes. Biomed Eng Online 17(Suppl 1):132.

6. Shi B (2021) Wearable exercise monitoring equipment for physical exercise teaching process based on wireless sensor. Microprocess Microsyst 81**:**103791.
7. Peng X, Dong K, Ye CY et al (2020) A breathable, biodegradable, antibacterial, and self-powered electronic skin based on all-nanofiber triboelectric nanogenerators. Sci Adv 6: eaba9624.
8. Yuan Y, Liu M, Tai WC, Zuo L (2017) Design and Treadmill Test of a Broadband Energy Harvesting Backpack With a Mechanical Motion Rectifier. J Mech Des 140(8): 085001.
9. Ren LM, Cong MY et al (2021) Harvesting the negative work of an active exoskeleton robot to extend its operating duration. Energy Convers Manag 245: 114640.
10. Mi J, Li QF et al (2020) Design, modelling, and testing of a vibration energy harvester using a novel half-wave mechanical rectification. Appl Energy 279: 115726.
11. Martin JP, Li QG (2017) Overground vs. treadmill walking on biomechanical energy harvesting: An energetics and EMG study. Gait Posture 52: 124-128.
12. Ylli K, Hoffmann D, Willmann A, et al (2015) Energy harvesting from human motion: exploiting swing and shock excitations. Smart Mater Struct 24(2): 025029-025029.
13. Berdy DF, Valentino DJ et al (2015) Kinetic energy harvesting from human walking and running using a magnetic levitation energy harvester. Sensor Actuat A-Phys 222: 262-271.
14. Kuang Y, Ruan T, Chew ZJ, et al (2017) Energy harvesting during human walking to power a wireless sensor node. Sensor Actuat A-Phys 254: 69-77.
15. Guan D, Jing XJ, Shen H et al (2019) Test and simulation the failure characteristics of twin tube shock absorber. Mech Syst Signal Pr 122: 707-719.
16. Guan D, Liu R, Fei CW et al (2020) Fluid-Structure Coupling Model and Experimental Validation of Interaction Between Pneumatic Soft Actuator and Lower Limb. Soft Robot 7(5): 627-638.
17. Guan D, Yang N, Lai J, et al (2021) Kinematic modeling and construction analysis for robotic excavator operation in piling construction. Automat Constr 126: 103666.
18. Li M, Jing XJ (2019) Novel tunable broadband piezoelectric harvesters for ultralow-frequency bridge vibration energy harvesting. Appl Energy 255(C): 113829-113829.
19. Wei CF, Jing XJ (2017) A comprehensive review on vibration energy harvesting: Modelling and realization. J Renew Sustain Energy 74: 1-18.
20. Saha CR et al (2008) Electromagnetic generator for harvesting energy from human motion. Sensor Actuat A-Phys 147(1):248-253.
21. Pan DH, Liu JX et al (2013) Analysis and Modeling of Eddy Current Damping for Short-Stroke DC Linear Motor. Appl Mech Mater 2698(416-417): 300—304.
22. Guan D, Cong XJ et al (2022) Experimental test and theoretical modeling on the working characteristics of spherical water pump. Flow Meas Instrum 85: 102162.
23. Guan D, Xu GQ et al (2021) Boosting the Output Performance of the Triboelectric Nanogenerator through the Nonlinear Oscillator. ACS Appl Mater Interfaces 13(5): 6331-6338.
24. Guan D, Cong XJ, Li J et al (2021) Quantitative characterization of the energy harvesting performance of soft-contact sphere triboelectric nanogenerator. Nano Energy, 87: 106186.
25. Gang XC, Guo ZH et al (2021) Textile Triboelectric Nanogenerators Simultaneously Harvesting Multiple 'High-Entropy' Kinetic Energies. ACS Appl Mater Interfaces 13(17): 20145–20152.
26. Guan D, Li J et al (2022) Theoretical modeling and optimal matching on the damping property of mechatronic shock absorber with low speed and heavy load capacity. J Sound Vib 535: 117113.